Choice of blood rheology model has minor impact on computational assessment of shear stress mediated vascular risk

By Miguel O. Bernabeu[1,2], Rupert W. Nash[1], Derek Groen[1], Hywel B. Carver[1,2], James Hetherington[3], Timm Krüger[1], Peter V. Coveney[1]

[1]Centre for Computational Science, Department of Chemistry, University College London, 20 Gordon Street, London, WC1H 0AJ, UK

[2]CoMPLEX, University College London, Physics Building, Gower Street, London, WC1E 6BT, UK

[3]Research Software Development Team, Research Computing and Facilitating Services, University College London, Podium Building - 1st Floor, Gower Street, London, WC1E 6BT, UK

Perturbations to the homeostatic distribution of mechanical forces exerted by blood on the endothelial layer have been correlated with vascular pathologies including intracranial aneurysms and atherosclerosis. Recent computational work suggests that in order to correctly characterise such forces, the shear-thinning properties of blood must be taken into account. To the best of our knowledge, these findings have never been compared against experimentally observed pathological thresholds. In the current work, we apply the three-band diagram (TBD) analysis due to Gizzi *et al.* to assess the impact of the choice of blood rheology model on a computational model of the right middle cerebral artery. Our results show that the differences between the wall shear stress predicted by a Newtonian model and the well known Carreau-Yasuda generalized Newtonian model are only significant if the vascular pathology under study is associated with a pathological threshold in the range $0.94\,\mathrm{Pa}$ to $1.56\,\mathrm{Pa}$, where the results of the TBD analysis of the rheology models considered differs. Otherwise, we observe no significant differences.

Keywords: Blood flow modelling, rheology, multiscale modelling, lattice-Boltzmann, three-band diagram analysis

1. Introduction

Physiology and medicine are being revolutionized by the growing role of information technology. Our ability to acquire and manage data on both animals and humans allows us to develop increasingly detailed computational models of the biological processes sustaining life. These models, together with the relevant experimental data, are helping researchers to gain insight into the physiology and pathology of the systems under study, in many cases beyond what is possible with purely observational methods.

Cerebrovascular disorders, including intracranial aneurysms (ICA), which may rupture leading to subarachnoid haemorrhages, are one of the most prevalent and devastating diseases of adults, of worldwide concern. In the UK, the total burden has been estimated as £0.5 billion annually [Rivero-Arias et al., 2010]. It is

currently generally accepted that haemodynamics plays an important role in the appearance, evolution, and potential rupture of these type of vascular pathologies [Stehbens, 1989, Shojima et al., 2004]. More precisely, perturbations in the homeostatic distribution of mechanical forces exerted by the blood on the endothelial layer have been correlated not only to aneurysm initiation and rupture but also to the development of other vascular pathologies such as atherosclerosis [Chatzizisis et al., 2008].

From a rheological point of view, blood is a shear-thinning fluid. This behaviour arises from the presence of red blood cells suspended in a medium known as blood plasma. Despite this fact, a large body of literature concerning computational haemodynamics characterises blood as a Newtonian fluid under the assumption that in large arteries the shear rate is large enough for the viscosity to be treated as effectively constant [Mejia et al., 2011].

There has been increasing interest during recent years in the comparison of blood rheology models using computational fluid dynamics (CFD) simulations in realistic computational domains reconstructed from medical image. These studies have been performed in both healthy vasculature (see *e.g.* [Morbiducci et al., 2011, Box et al., 2005, Johnston et al., 2004]) and in the presence of aneurysms (see *e.g.* [Bernsdorf and Wang, 2009, Cavazzuti et al., 2011, Fisher and Rossmann, 2009]). In particular, authors pay special attention to the influence of the choice of rheology model on the computational estimates of wall shear stress (WSS) as a proxy for aneurysm rupture risk. It has been suggested that, in ICAs, the Newtonian simplification overestimates WSS (see *e.g.* [Bernsdorf and Wang, 2009, Xiang et al., 2012]) and may underestimate rupture risk. Furthermore, it has been argued that applications requiring accurate WSS estimates (*e.g.* those concerning vascular remodelling and biomechanics) will suffer from modelling inaccuracy unless the generalized Newtonian (GN) properties of blood are taken into account.

Different indices have been proposed as a way of integrating into CFD-based biomarkers of rupture risk the rich spatio-temporal structure of WSS induced by pulsatile flow in complex vascular networks. Minimal or maximal peak WSS, time-averaged WSS, and oscillatory shear index (OSI) [Ku et al., 1985] have been extensively used, among others. In many of the studies cited previously, comparisons are performed based on colour map plots, of one or more of these indices, on the surface of the original computational domain. Differences between WSS estimates produced by different rheology models are hence presented in a very qualitative way. Furthermore, the link to actual rupture risk is based on the currently accepted low shear stress biomarker, but with no actual correlation to experimentally determined WSS thresholds. Several authors [Kallmes, 2012, Cebral and Meng, 2012] have recently criticised this approach to rupture risk quantification arguing that more quantitative methods are required in order to gain further insight into the problem.

In a recent publication, Gizzi *et al.* [Gizzi et al., 2011] proposed a new framework for the quantitative analysis of WSS: the so-called three-band diagram (TBD) analysis. The TBD analysis facilitates the evaluation of the WSS obtained at a given location over time (*i.e.* a WSS signal) against a range of WSS pathological thresholds (*e.g.* WSS magnitude lower than 0.5 Pa as reported in the case of atherosclerosis formation [Chatzizisis et al., 2008]). The analysis determines how likely a given WSS signal is to be considered risky for any given threshold. Further-
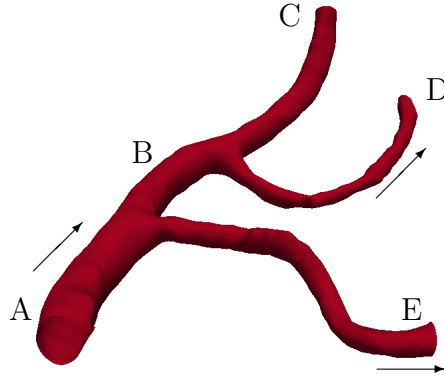
Figure 1. 3D model of a subset of the right middle cerebral artery used in this work. Geometry segments are numbered A–E for later reference. The arrows indicate flow direction.

more, the results of the analysis can be easily compared against pathological values of WSS observed experimentally.

In the current work, we apply TBD analysis to assess the impact of the choice of blood rheology model on the WSS estimates of the HEMELB [Mazzeo and Coveney, 2008] lattice-Boltzmann blood flow solver in a high resolution three-dimensional model of the right middle cerebral artery. The rest of the paper is structured as follows: §2 introduces the computational and mathematical models used in this work as well as the simulation workflow implemented, §3 presents the results of our simulation and their main implications, finally §4 summarises the main conclusions of the work and outlines future research directions.

2. Methods

(a) *3D model of the middle cerebral artery*

(i) *Geometry generation*

The three-dimensional (3D) model of the middle cerebral artery used in this work (see figure 1) is a subset of a geometrical model of the intracranial vasculature reconstructed from rotational angiography scans.It corresponds to a section of the right middle cerebral artery (MCA) in the vicinity of the internal carotid artery. The main geometrical features of the model are: i) vessels of variable diameter, ii) two bifurcations, and iii) vessel bending. The National Hospital for Neurology and Neurosurgery, London (UK) provided the original images in the framework of the GENIUS project [Mazzeo et al., 2010] as part of a larger dataset library. The dataset used in this work was segmented and the surface mesh in figure 1 generated with the open source package Vascular Modeling Toolkit (VMTK) [Antiga et al., 2008].

(ii) HemeLB

HemeLB [Mazzeo and Coveney, 2008] is an open source software platform† for modelling and simulation of blood flow in sparse vascular networks. It is comprised of tools for geometrical model preprocessing (*i.e.* regular grid volume meshing of surface meshes), simulation on massively parallel architectures, real-time visualization and steering, and data post-processing. To date, HemeLB has been successfully applied to the simulation of blood flow in healthy brain vasculature as well as in the presence of intracranial aneurysms. Particular attention has been paid to obtaining and presenting simulation results in a clinically meaningful way [Mazzeo et al., 2010]. HemeLB uses the lattice-Boltzmann method for fluid dynamics (see *e.g.* [Chen and Doolen, 1998]) since it allows efficient implementations in large-scale high performance computing infrastructures. For this work, we have developed an extension of HemeLB's lattice Bhatnagar-Gross-Krook (LBGK) collision operator in order to accommodate both Newtonian and GN rheology models. We use the D3Q15 velocity set and the halfway bounce-back rule [Chen and Doolen, 1998] to enforce the no-slip boundary condition at the walls. We have recently shown [Carver et al., 2012] that this combination of collision operator, velocity set, and wall boundary condition performs well from both a numerical and a computational point of view in complex domains for typical blood flow Reynolds and Womersley numbers.

(iii) *Generalized Newtonian rheology*

The Carreau-Yasuda (CY) model is widely used to describe the shear-thinning behaviour of blood [Boyd et al., 2007, Ashrafizaadeh and Bakhshaei, 2009]. In this model, the dynamic viscosity η is related to the shear rate $\dot{\gamma}$ through the following expression:

$$\eta(\dot{\gamma}) = \eta_\infty + (\eta_0 - \eta_\infty)\left(1 + (\lambda\dot{\gamma})^a\right)^{\frac{n-1}{a}} , \tag{2.1}$$

where a, n, and λ are empirically determined to fit a curve between regions of constant η_∞ and η_0. This model defines three different regimes: a Newtonian region with η_0 for low shear rate, followed by a shear-thinning region where η decreases with $\dot{\gamma}$; finally, once η_∞ is reached a third Newtonian region with constant viscosity η_∞ is defined for high shear rates. In this work, we will use the values provided in [Boyd et al., 2007]: $\eta_0 = 0.16 \, \text{Pa}\,\text{s}$, $\eta_\infty = 0.0035 \, \text{Pa}\,\text{s}$, $\lambda = 8.2$ s, $a = 0.64$, and $n = 0.2128$ (both are dimensionless).

Figure 2 presents viscosity as a function of shear rate for the previous model and the Newtonian model considered in this work ($\eta = 3.5 \times 10^{-3} \, \text{Pa}\,\text{s}$). The Carreau-Yasuda model displays a smooth transition between η_0 and η_∞. Significant haemodynamic differences between the two rheology models are expected for simulations with $\dot{\gamma} < 100 \, \text{s}^{-1}$.

(b) *1D model of the human vascular system*

In order to obtain inlet and outlet boundary conditions for our 3D model, we use a modified version of a one-dimensional (1D) model of the human vascular system previously published in [Mulder et al., 2011]. The original model includes a 1D representation of the main arteries in the upper body (including the circle
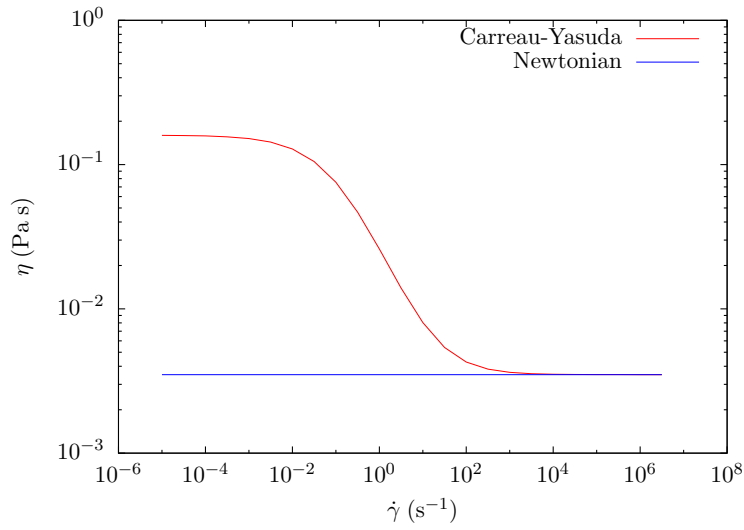
† The codebase is available under LGPL license from `http://ccs.chem.ucl.ac.uk/hemelb`.

Figure 2. Dynamic viscosity η as a function of shear rate $\dot{\gamma}$ for the Carreau-Yasuda (red) and the Newtonian (blue) models.

Table 1. *Geometrical characterisation of the 3D model used in this work.*

Segment	Length	Proximal end radius	Distal end radius
A	8.9 mm	1.30 mm	1.25 mm
B	11.2 mm	1.25 mm	1.10 mm
C	13.6 mm	1.10 mm	0.85 mm
D	20.6 mm	0.62 mm	0.62 mm
E	21.1 mm	0.77 mm	0.77 mm

of Willis and both MCAs) and a zero-dimensional representation of the peripheral vasculature. The geometry is available as part of the open source software package pyNS [Manini et al., 2012] which also implements a numerical solver for the 1D pulse propagation mathematical model presented in [Huberts et al., 2012].

The original 1D geometrical model does not include any detail about the vessels branching off the right MCA. Therefore, we modified it to include the two MCA side branches present in the 3D model (see figure 1). In order to achieve this a 1D characterisation of the 3D geometry was required. The open source software package VMTK was used to compute: a) the length of the centrelines associated with segments A–E in figure 1, and b) the radii of the maximum inscribed spheres along the centrelines. Table 1 summarises the results and figure 3 shows a schematic of the 1D model including the more detailed representation of the right MCA. The reader is referred to [Mulder et al., 2011] or the pyNS tool for the names and characteristics (*e.g.* length, radius, connectivity) of each of the segments of the vascular system.
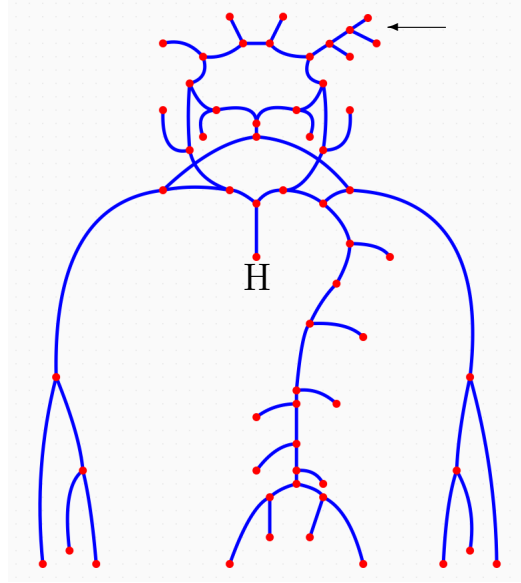
Figure 3. 1D model of the main arteries in the upper body. Each segment (in blue) represents a different part of a human arterial system including characterisation of the 3D model of the right MCA in figure 1 (see top right arrow). Segment lengths are not to scale. The red dots represent: i) bifurcations, when found at the intersection of two or more segments, ii) zero-dimensional representations of the peripheral vasculature, when found at the end of an open-ended segment or iii) the heart in the case labelled with H.

(c) Three-band diagram analysis

The extraction of synthetic biomarkers of aneurysm rupture risk based on CFD analysis of patient-specific models is an active field of research. The three-band diagram analysis framework was recently proposed [Gizzi et al., 2011] as a way of generalising previously proposed indices (*e.g.* time-averaged WSS, OSI) and providing a quantitative way of comparing temporal WSS signals against specific risk factors.

Let **t** be the instantaneous traction vector at an arbitrary surface point with associated surface unit normal $\hat{\mathbf{n}}$ such that

$$\mathbf{t}_i = \mathrm{T}_{ij}\hat{\mathbf{n}}_j \; , \tag{2.2}$$

where T is the deviatoric part of the full stress tensor of a fluid computed from the mesoscopic LB simulation variables as described in [Krüger et al., 2009]. The relationship between T and σ, the full stress tensor, is

$$\sigma_{ij} = -P\delta_{ij} + \mathrm{T}_{ij} \; , \tag{2.3}$$

where P is the hydrodynamic pressure and δ is the usual Kronecker delta tensor. Furthermore, for a generalized Newtonian incompressible fluid, T can be rewritten as

$$\mathrm{T}_{ij} = 2\eta(\dot{\gamma})\mathrm{S}_{ij} \; , \tag{2.4}$$

where S is the shear rate tensor

$$\mathrm{S}_{ij} = \frac{1}{2}(\partial_i v_j + \partial_j v_i) \,, \tag{2.5}$$

η is the dynamic viscosity of a fluid as a function of shear rate $\dot{\gamma} = \sqrt{2S_{ij}S_{ij}}$, see *e.g.* equation (2.1), and $\mathbf{v}$ is the velocity vector. In the case of Newtonian fluids, $\eta(\dot{\gamma}) = \eta = \mathrm{const.}$

In this work, we will consider the temporal evolution of the signed magnitude of the traction vector $\mathbf{t}$ (which we will refer as the WSS signal), *i.e.*:

$$S(t) \coloneqq \mathrm{sgn}(\mathbf{t}(t) \cdot \bar{\mathbf{t}})|\mathbf{t}(t)| \,, \tag{2.6}$$

where $\bar{\mathbf{t}}$ is the average traction vector over time, sgn is the sign function, and $|\cdot|$ is the magnitude of a given vector.

Given a WSS signal, $S(t)$, and a scalar risk factor $\sigma \geq 0$, the TBD analysis defines a triplet of functions

$$
\begin{aligned}
S^+(t) &\coloneqq S(t)H(S(t) - \sigma), \\
S^0(t) &\coloneqq S(t)H(\sigma - S(t))H(\sigma + S(t)), \\
S^-(t) &\coloneqq S(t)H(-S(t) - \sigma),
\end{aligned}
\tag{2.7}
$$

where the Heaviside function $H(x)$ is defined as $H(x) = 1$ if $x > 0$ and $H(x) = 0$ if $x < 0$. The closed support of the function S^+ is a set of time intervals of cardinality $N^+(\sigma)$ (and similarly with S^0 and S^-). The main idea behind the method is to inspect the number of such intervals as a function of the variable threshold σ (*i.e.* the risk factor). It has been suggested that a WSS signal can be considered healthy if $N^{+,0,-}(\sigma) > 0$ for a given risk factor σ. The reader is referred to [Gizzi et al., 2011] for a more detailed description of the method. A Python implementation of the algorithm is freely available as part of HEMELB's postprocessing tools.

(d) *Simulation workflow*

Our simulation workflow is as follows. First, the original DICOM images were segmented, a region of interest was chosen, and a surface mesh was generated with the VMTK implementation of the marching cubes algorithm. A non-shrinking Taubin filter was then applied to smooth out imaging artifacts. Second, we loaded the resulting surface mesh in HEMELB's setup tool in order to choose the location of the inlet and the outlets and generate a regular grid discretisation of the volume enclosed by the surface (with a total of 4,161,046 grid points). Next, the pyNS solver was run to obtain pressure traces at inlet A and oulets C–E in figure 3. We then used these traces as inlet and outlet boundary conditions to run HEMELB simulations with both the Newtonian and Carreau-Yasuda rheology models for a total of three cardiac cycles. The following configuration paremeters were used in this work: timestep $\Delta t = 2.5706 \times 10^{-6}$ s, spacestep $\Delta x = 3.50 \times 10^{-5}$ m, maximum density difference in the domain $\Delta\rho/\rho_0 = 0.019$, Mach numbers (defined as the ratio between the largest velocity magnitude in the domain and lattice speed of sound $c_s = \frac{\Delta x}{\sqrt{3}\Delta t}$) 0.31 and 0.244 for the Newtonian and CY rheology models respectively, and LBGK relaxation parameter $\tau = 0.522$ for the Newtonian model

Table 2. *Three-band diagram analysis sampling points.*

Point	Coordinates
x_1	(11.38, 36.89, 45.17) mm
x_2	(10.98, 41.64, 47.97) mm
x_3	(12.77, 41.15, 45.02) mm
x_4	(12.34, 42.69, 46.17) mm
x_5	(11.88, 50.29, 41.31) mm
x_6	(11.59, 50.55, 49.19) mm
x_7	(12.89, 55.45, 44.75) mm
x_8	(12.82, 55.33, 45.58) mm
x_9	(14.57, 55.73, 52.63) mm

and $\tau = \frac{1}{2} + \frac{\eta(\dot{\gamma})}{\Delta t c_s^2 \rho}$ for the CY model (which becomes $\tau = 0.522$ for η_∞). Finally, we post-processed the simulation results to compute TBDs of the WSS signal at different geometrical locations over time. Table 2 shows their location for reproducibility purposes.

The pyNS simulations were run on a single core of a 2 GHz Intel Core i7 laptop with 4GB of RAM and took on the order of minutes to run. The HemeLB simulations were run on 2048 cores of HECToR (UK's national supercomputer) and took 53 min and 83 min for the Newtonian and Carreau-Yasuda models respectively. The difference in computing time between the two rheology models is due to the cost associated with computing $\dot{\gamma}$ and evaluating equation (2.1) at each lattice site every timestep. The choice of core count is based on the number of lattice sites and the scalability analysis presented in [Groen et al., 2012b] in order to ensure efficient use of the computational resources.

All the files required to run the pyNS and HemeLB simulations are available as part of the supplementary material associated with this paper. Both software packages are open source and freely available to the public.

3. Results and discussion

(a) Pressure profiles

Figure 4 plots the pressure traces generated by pyNS at inlet A and outlets C–E of figure 3. It can be seen how the typical pressure variations observed throughout the cardiac cycle are well recovered. First, the sudden increase in pressure following the opening of the aortic valve after approximately 0.06 s, which peaks at around 0.2 s and drops until approximately 0.4 s corresponds to the ventricular ejection phase. Secondly, the isovolumic relaxation phase happens between the previous time point and the mitral valve opening around 0.55 s. Finally, the ventricular filling phase occurs between the time the mitral valve opens and the end of the cycle at approximately 0.91 s (for a cardiac rate of roughly 66 beats per minute).

(b) 3D simulations and three-band diagram analysis

Figure 5 plots the traction vector **t** computed with HemeLB configured to use the CY rheology model at the end of diastole and at peak flow in systole (both in the third cardiac cycle simulated). The direction of **t** (which is consistent with the flow direction at any given point) and its magnitude follow a complex distribution

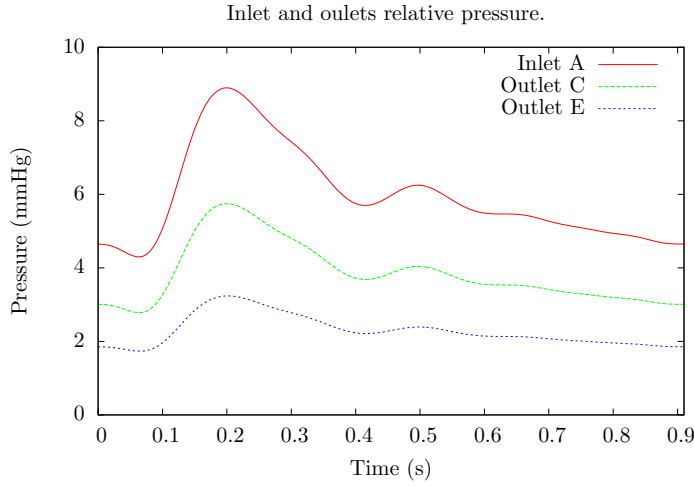Inlet and oulets relative pressure.

Figure 4. Pressure profiles at the inlet and outlets obtained from the 1D model. Pressures are displayed relative to outlet D. Simulations were run for a total of three cardiac cycles.

throughout the domain with notable changes during the cardiac cycle. The main characteristics are: i) areas with larger WSS can be found in the interior side of both branches leaving the bifurcation, ii) a zone of low WSS, or stagnation point, is found around the area where both branches meet, iii) there are substantial changes in the direction of $\mathbf{t}$ throughout the cardiac cycle around the stagnation point area, leading to oscillatory WSS signals.

Figure 6 presents the TBD analysis at points x_3, x_4, and x_5. The analysis confirms the change of sign of the WSS signal (due to a change of direction in the traction field) occurring at x_4 throughout the cardiac cycle (note the presence of a negative component in figures 6(c) and 6(d)). Furthermore, the negative component covers a wider range of threshold values in the Newtonian case. According to the criteria outlined in [Gizzi et al., 2011], an oscillatory WSS signal is considered healthy when the TBD analysis displays all three components above a given critical threshold. In this case we observe a variation of just over $0.5\,\mathrm{Pa}$ between the predicted largest healthy threshold in the Newtonian and CY cases.

In the case of x_3 and x_5 no negative component appears in the analysis indicating that there is no oscillation in the WSS signal. This rules out one of the main factors correlated with vascular disorders: oscillatory flow [Ku et al., 1985]. Nevertheless, such signals could still be considered risky if their mean value was below a given threshold value [Shojima et al., 2004]. We can clearly see in figures 6(a)–6(b) and 6(e)–6(f) that the choice of rheology model would not have a significant impact on the assessment of risk since both diagrams are nearly identical.

The points listed in table 2 which have not been analysed in figure 6 fall within one of the two previous scenarios.

4. Conclusions

In this work, we present a complete workflow for the simulation of blood flow in a patient-specific 3D model of the right middle cerebral artery. The main features of
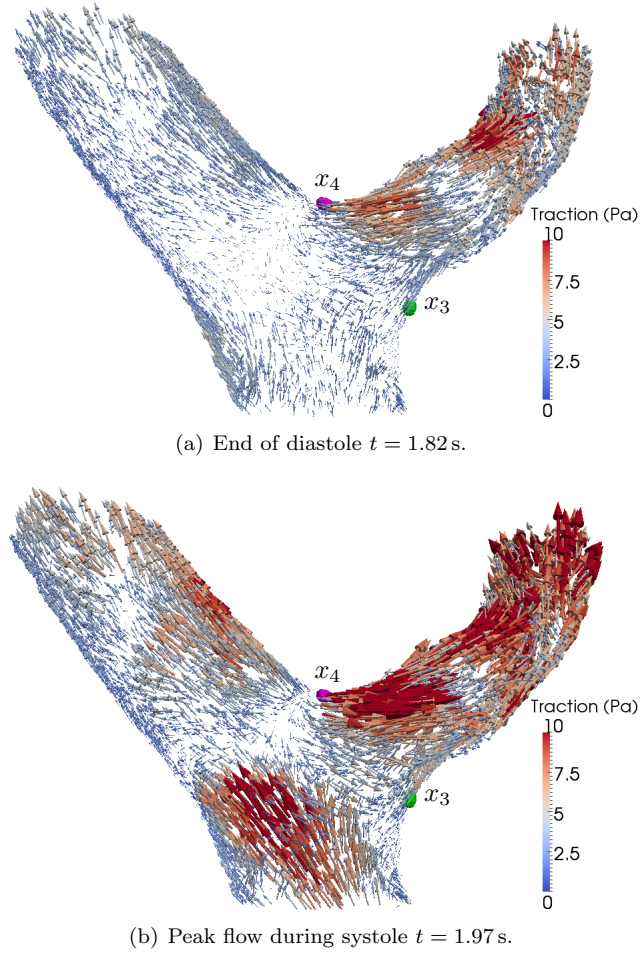
(a) End of diastole $t = 1.82$ s.

(b) Peak flow during systole $t = 1.97$ s.

Figure 5. Traction vector **t** (estimated with the CY rheology model) at the upstream bifurcation of the 3D model. Vectors are scaled according to their magnitude. Points x_3 and x_4 in table 2 are shown in green and magenta respectively. Visualizations generated with the open source software package Paraview [Henderson, 2007].

the model are: i) the geometry is reconstructed from rotational angiography scans and discretised at high resolution ($\Delta x = 3.5 \times 10^{-5}$ m), ii) inlet and outlet boundary conditions are obtained with a 1D model of the complete vascular system, and iii) the rheological properties of the blood can be described with both Newtonian and generalized Newtonian models. Simulations run efficiently on the HECToR supercomputer taking 53 min to 83 min for a domain comprising of 4,161,046 lattice sites.

The workflow is applied to the comparison of two blood rheology models: a Newtonian model ($\eta = 3.5 \times 10^{-3}$ Pa s) and the Carreau-Yasuda (CY) model. This is done in a quantitative manner in conjunction with the recently proposed three-band diagram (TBD) analysis framework. In agreement with previous work (see *e.g.* [Morbiducci et al., 2011, Bernsdorf and Wang, 2009]), our results show variations in the haemodynamics recovered with each of the rheology models studied. However,
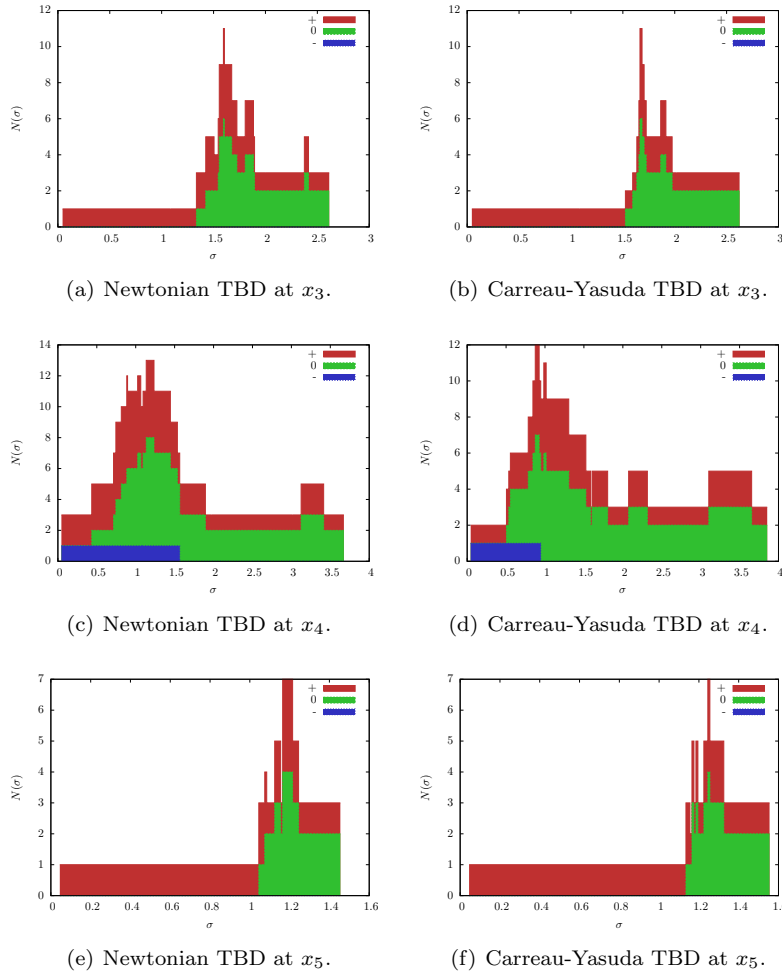
(a) Newtonian TBD at x_3.

(b) Carreau-Yasuda TBD at x_3.

(c) Newtonian TBD at x_4.

(d) Carreau-Yasuda TBD at x_4.

(e) Newtonian TBD at x_5.

(f) Carreau-Yasuda TBD at x_5.

Figure 6. TBD analysis at points x_3, x_4, and x_5. The values of $N^{\{-,0,+\}}(\sigma)$ are presented as a stacked histogram.

the evaluation of those results against a set of risk factors with TBD show little to no difference. In particular, a wall shear stress signal with strong oscillatory component was found to be risky for thresholds equal to or greater than 1.56 and 0.94 Pa for the Newtonian and CY models respectively. In the case of non-oscillatory signals the analysis returns almost identical results in both cases.

The main limitations of our study are: i) we have used a single geometry; in order to achieve statistical significance a larger number of other cases must be considered, and ii) the results presented may not hold in the presence of intracranial aneurysms (ICAs) or other vascular malformations where regions of much smaller shear rate may occur.

Our future lines of work include applying the analysis methodology presented in the current work to a set of ICAs reconstructed from rotational angiography images. We also plan to investigate the coupling of the current 1D-3D haemodynamics

model with agent-based models of tissue remodelling using the multiscale modelling framework presented in [Groen et al., 2012a].

Acknowledgements

References

[Antiga et al., 2008] Antiga, L., Piccinelli, M., Botti, L., Ene-Iordache, B., Remuzzi, A., and Steinman, D. (2008). An image-based modeling framework for patient-specific computational hemodynamics. *Medical & Biological Engineering & Computing*, 46:1097–1112.

[Ashrafizaadeh and Bakhshaei, 2009] Ashrafizaadeh, M. and Bakhshaei, H. (2009). A comparison of non-newtonian models for lattice boltzmann blood flow simulations. *Comput. Math. Appl.*, 58:1045–1054.

[Bernsdorf and Wang, 2009] Bernsdorf, J. and Wang, D. (2009). Non-newtonian blood flow simulation in cerebral aneurysms. *Comput. Math. Appl.*, 58(5):1024–1029.

[Box et al., 2005] Box, F. M. A., van der Geest, R. J., Rutten, M. C. M., and Reiber, J. H. C. (2005). The influence of flow, vessel diameter, and non-newtonian blood viscosity on the wall shear stress in a carotid bifurcation model for unsteady flow. *Invest Radiol*, 40(5):277–294.

[Boyd et al., 2007] Boyd, J., Buick, J. M., and Green, S. (2007). Analysis of the casson and carreau-yasuda non-newtonian blood models in steady and oscillatory flows using the lattice boltzmann method. *Physics of Fluids*, 19(9):093103.

[Carver et al., 2012] Carver, H. B., Nash, R. W., Bernabeu, M. O., Hetherington, J., Groen, D., Krüger, T., and Coveney, P. V. (2012). Choice of boundary condition and collision operator for lattice-Boltzmann simulation of moderate Reynolds number flow in complex domains. *ArXiv e-prints 1211.0205*.

[Cavazzuti et al., 2011] Cavazzuti, M., Atherton, M. A., Collins, M. W., and Barozzi, G. S. (2011). Non-newtonian and flow pulsatility effects in simulation models of a stented intracranial aneurysm. *Proceedings of the Institution of Mechanical Engineers, Part H: Journal of Engineering in Medicine*, 225(6):597–609.

[Cebral and Meng, 2012] Cebral, J. and Meng, H. (2012). Counterpoint: Realizing the clinical utility of computational fluid dynamics—closing the gap. *American Journal of Neuroradiology*, 33(3):396–398.

[Chatzizisis et al., 2008] Chatzizisis, Y. S., Jonas, M., Coskun, A. U., Beigel, R., Stone, B. V., Maynard, C., Gerrity, R. G., Daley, W., Rogers, C., Edelman, E. R., Feldman, C. L., and Stone, P. H. (2008). Prediction of the localization of high-risk coronary atherosclerotic plaques on the basis of low endothelial shear stress. *Circulation*, 117(8):993–1002.

[Chen and Doolen, 1998] Chen, S. and Doolen, G. (1998). Lattice boltzmann method for fluid flows. *Ann. Rev. Fluid Mech*, (30):329–364.

[Fisher and Rossmann, 2009] Fisher, C. and Rossmann, J. (2009). Effect of non-newtonian behavior on hemodynamics of cerebral aneurysms. *Journal of biomechanical engineering*, 131(9):091004.

[Gizzi et al., 2011] Gizzi, A., Bernaschi, M., Bini, D., Cherubini, C., Filippi, S., Melchionna, S., and Succi, S. (2011). Three-band decomposition analysis of wall shear stress in pulsatile flows. *Phys. Rev. E*, 83:031902.

[Groen et al., 2012a] Groen, D., Borgdorff, J., Bona-Casas, C., Hetherington, J., Nash, R. W., Zasada, S. J., Saverchenko, I., Mamonski, M., Kurowski, K., Bernabeu, M. O., Hoekstra, A. G., and Coveney, P. V. (2012a). Flexible composition and execution of high performance, high fidelity multiscale biomedical simulations. *ArXiv e-prints 1211.2963*.

[Groen et al., 2012b] Groen, D., Hetherington, J., Carver, H. B., Nash, R. W., Bernabeu, M. O., and Coveney, P. V. (2012b). Analyzing and Modeling the Performance of the HemeLB Lattice-Boltzmann Simulation Environment. *ArXiv e-prints 1209.3972*.

[Henderson, 2007] Henderson, A. (2007). *The ParaView Guide: A Parallel Visualization Application*. Kitware Inc.

[Huberts et al., 2012] Huberts, W., Bode, A., Kroon, W., Planken, R., Tordoir, J., van de Vosse, F., and Bosboom, E. (2012). A pulse wave propagation model to support decision-making in vascular access planning in the clinic. *Medical Engineering & Physics*, 34(2):233 – 248.

[Johnston et al., 2004] Johnston, B. M., Johnston, P. R., Corney, S., and Kilpatrick, D. (2004). Non-newtonian blood flow in human right coronary arteries: steady state simulations. *Journal of Biomechanics*, 37(5):709 – 720.

[Kallmes, 2012] Kallmes, D. (2012). Point: Cfd—computational fluid dynamics or confounding factor dissemination. *American Journal of Neuroradiology*, 33(3):395–396.

[Krüger et al., 2009] Krüger, T., Varnik, F., and Raabe, D. (2009). Shear stress in lattice boltzmann simulations. *Phys. Rev. E*, 79:046704.

[Ku et al., 1985] Ku, D. N., Giddens, D. P., Zarins, C. K., and Glagov, S. (1985). Pulsatile flow and atherosclerosis in the human carotid bifurcation. positive correlation between plaque location and low oscillating shear stress. *Arteriosclerosis, Thrombosis, and Vascular Biology*, 5(3):293–302.

[Manini et al., 2012] Manini, S., Antiga, L., Huberts, W., Botti, L., and Remuzzi, A. (2012). pyns, an open source framework for 0d/1d hemodynamic modelling. In *10th International Symposium on Biomechanics and Biomedical Engineering*.

[Mazzeo and Coveney, 2008] Mazzeo, M. D. and Coveney, P. V. (2008). HemeLB: A high performance parallel lattice-Boltzmann code for large scale fluid flow in complex geometries. *Computer Physics Communications*, pages 894–914.

[Mazzeo et al., 2010] Mazzeo, M. D., Manos, S., and Coveney, P. V. (2010). In situ ray tracing and computational steering for interactive blood flow simulation. *Computer Physics Communications*, 181(2):355–370.

[Mejia et al., 2011] Mejia, J., Mongrain, R., and Bertrand, O. F. (2011). Accurate Prediction of Wall Shear Stress in a Stented Artery: Newtonian Versus Non-Newtonian Models. *Journal of Biomechanical Engineering*, 133(7):074501+.

[Morbiducci et al., 2011] Morbiducci, U., Gallo, D., Massai, D., Ponzini, R., Deriu, M. A., Antiga, L., Redaelli, A., and Montevecchi, F. M. (2011). On the importance of blood rheology for bulk flow in hemodynamic models of the carotid bifurcation. *Journal of Biomechanics*, 44(13):2427 – 2438.

[Mulder et al., 2011] Mulder, G., Bogaerds, A., Rongen, P., and van de Vosse, F. (2011). The influence of contrast agent injection on physiological flow in the circle of willis. *Medical Engineering & Physics*, 33(2):195 – 203.

[Rivero-Arias et al., 2010] Rivero-Arias, O., Gray, A., and Wolstenholme, J. (2010). Burden of disease and costs of aneurysmal subarachnoid haemorrhage (asah) in the united kingdom. *Cost Effectiveness and Resource Allocation*, 8(6).

[Shojima et al., 2004] Shojima, M., Oshima, M., Takagi, K., Torii, R., Hayakawa, M., Katada, K., Morita, A., and Kirino, T. (2004). Magnitude and role of wall shear stress on cerebral aneurysm. *Stroke*, 35(11):2500–2505.

[Stehbens, 1989] Stehbens, W. E. (1989). Etiology of intracranial berry aneurysms. *Journal of Neurosurgery*, 70(6):823–831.

[Xiang et al., 2012] Xiang, J., Tremmel, M., Kolega, J., Levy, E. I., Natarajan, S. K., and Meng, H. (2012). Newtonian viscosity model could overestimate wall shear stress in intracranial aneurysm domes and underestimate rupture risk. *Journal of NeuroInterventional Surgery*, 4(5):351–357.